Molecular dynamics simulations of crystal nucleation in entangled polymer melts under start-up shear conditions

Muhammad Anwar[1, a)] and Richard S. Graham[1]

School of Mathematical Sciences, University of Nottingham, Nottingham NG7 2RD, United Kingdom

(Dated: 1 February 2019)

Understanding the flow induced crystallisation (FIC) process is necessary due to its technological relevance to polymer processing. Polymer crystallisation controls the morphology of semi-crystalline polymers and hence the properties of the end product. We perform molecular dynamics simulations of polymer melts consisting of sufficiently entangled linear chains under shear flow. We determine the Rouse relaxation time (τ_{R}) for linear polymer chains using an established rheological model at different temperatures and fit the simulation data with the Arrhenius and Williams-Landel-Ferry (WLF) equations. We simulate the crystallisation induction times for different values of the Rouse Weissenberg number ($\mathrm{W_{iR}} = \dot{\gamma}\tau_R$) at different temperatures. We observe that the level of strain and stretch required to induce crystallisation increases with temperature. We find that the induction times follow a power law in shear rate and observe a more pronounced effect of flow rate for higher temperatures than at lower temperatures. Moreover, we determine that nucleation events occur relatively early in the shear transient and at a stretch value that is smaller than its steady state value. We also report the values of strain at which the occurrence of a nucleation event is most likely to happen.

I. INTRODUCTION

The commercial importance of polymer processing means that polymer crystallisation remains an active and vital field even after extensive efforts over several decades from various fields of science, engineering and technology. This topic is not only interesting scientifically but its understanding is also necessary for industry to produce products of desired mechanical, thermal and optical properties. Polymer crystallisation defines the morphology of semi-crystalline polymers, which has a strong influence on many of the properties of the end product. Therefore, in order to achieve the desired product properties, we must have better control over the crystallisation process in order to select the morphology of these materials. This requires a thorough understanding of the crystallisation process.

It is well known that flow enhances nucleation and affects the morphology of the crystallites. Commercially, polymer melts pass through fast shear or extensional flows during processing. Experimentally, intensive efforts have been made to understand the crystallisation process under quiescent conditions[1–10] and under the influence of external flow[11–23]. In these studies, the flow affects the nucleation and growth rates and morphological features including single and multiple shish. Key factors in this effect are the molecular weight distribution, molecular architecture and relaxation times. Theoretically, the non-equilibrium nature of flow induced crystallisation makes the problem enormously difficult. There are coarse grained semi-empirical models available,[15,24–32]. While these models contain partial microscopic information and some arguments to describe the experimental phenomenon, the coupling between the underlying stochastic processes is oversimplified. Consequently, they can not predict the dependence of the nucleation rate on temperature or molecular weight.

Experimentally, it is extremely difficult to detect flow induced crystallisation at its earliest stage because the small spatio-temporal scales are below the resolution of available experimental techniques[33]. In such scenarios, computer simulations are a good candidate to investigate the problem. On a mesoscopic level, kinetic Monte Carlo[34] simulations have been performed and the effects of shear rate, shear time and shear strain on the crystallisation kinetics, morphology and rheology have been discussed. Graham and Olmsted[35,36] have developed a coarse-grained kinetic Monte Carlo model. It can capture many features of flow induced crystallisation and is able to reproduce the effect of flow rate on crystallisation kinetics, which is in a good agreement with experimental data. However, it is a phenomenological model which makes pre-assumptions about the nucleus shape and relies on unknown thermodynamic parameters. Therefore there is a strong need for detailed molecular simulations with full resolution down to the monomer scale. On a molecular level, Monte Carlo (MC) and molecular dynamics (MD) simulations have been performed to address polymer crystallisation under quiescent conditions[37–60] and under flow or large deformation[61–70]. More recently, Graham[71] has reviewed and discussed the recent advances and future directions for a better understanding of FIC, with an emphasis on the role of molecular simulations. This review covers advantages, disadvantages and limitation of experiments, theory and multiscale simulations of FIC. In the case of flow induced crystallisation, there are very few MD studies[70,72] that quantify flow in-

a)manwar18@gmail.com

duced nucleation. These studies focused on short chain alkanes of length 20 monomers and 150 monomers. They reported the nucleation mechanism and kinetics for these short chains. However, longer chains that are sufficiently entangled have not been investigated yet using molecular dynamics simulations. Therefore, in this work, we report flow induced crystallisation of linear polymer chains consisting of 1000 monomers (entanglements ~ 13) under different degrees of super-cooling (4-14%) and at different values of the Rouse Weissenberg number (20-80). Another distinct feature of this work is that we use a rheological model to contextualise our data, because flow induced crystallisation and polymer rheology are strongly linked.

II. METHODOLOGY

A. Model

We use a united atom model, which has been used extensively by Rutledge and co-workers[41–43,70] and Schilling and co-workers[45,72,73] to study crystallisation under quiescent and under flow conditions. This model was proposed by Paul et.al.[74] and then modified by Waheed et.al[56]. In this model, CH_2 and CH_3 groups are represented by beads or "united atoms". These beads interact with each other via bonded and nonbonded potentials. The nonbonded interaction consists of Lennard Jones interactions and can be expressed by following relation for a distance r_{ij} between monomers i and j:

$$U(r_{ij}) = 4\epsilon_{ij}[(\frac{\sigma_{ij}}{r_{ij}})^{12} - (\frac{\sigma_{ij}}{r_{ij}})^{6}], r_{ij} \leq 2.5\sigma_{ij}$$
$$U(r_{ij}) = 0, r_{ij} > 2.5\sigma_{ij}. \quad (1)$$

The bonded potential, which acts between monomers along the chain, consists of a harmonic bond potential

$$U(r_{ij}) = \frac{1}{2}K(r_{ij} - R)^2, \quad (2)$$

a harmonic bond angle potential

$$U(\theta) = \frac{1}{2}K_\theta(\theta - \theta_0)^2, \quad (3)$$

where θ is the angle between two consecutive bonds, and a dihedral potential

$$U(\phi,) = \frac{1}{2}[K_{1\phi}(1-\cos\phi)+K_{2\phi}(1-\cos 2\phi)+K_{3\phi}(1-\cos 3\phi)] \quad (4)$$

where ϕ is the dihedral angle defined by three consecutive bonds.

We provide parameters for all potentials in Table I. The model has been optimised to reproduce the dynamical and structural properties of the melt, the melting point, and the rotator phase properties.

TABLE I: Parameters for the model: all parameters have been taken from[75], except for the Lennard Jones cutoff radius which is from[41].

Potential	Parameters
Harmonic bond	bond length = 1.53 A° K = 700 kcal/mol $A^{\circ 2}$
Bond Angle	K_θ = 120 kcal/mol θ_0 = 109.5 $^\circ$
Dihedral	$K_{1\phi}$ = 1.6 kcal/mol $K_{2\phi}$ = -0.867 kcal/mol $K_{3\phi}$ = 3.24 kcal/mol
Lennard Jones	σ = 4.01 A° ϵ $(CH_2 - CH_2)$ = 0.112 kcal/mol ϵ $(CH_3 - CH_3)$ = 0.112 kcal/mol ϵ $(CH_2 - CH_3)$= 0.112 kcal/mol Cut off = 2.5 σ

B. Order parameters

In order to identify the crystalline regions within a melt, we use a crystallinity order parameter that has been used recently by Schilling and co-workers[45,72,73]. This order parameter is based on the local alignment of segments of chains.

- First of all, we identify the neighbouring particles j of a given particle i, which lie within a cut-off radius of $r_c = 1.5\sigma$ from particle i, with particle i and j not on the same chain.
- We associate a unit vector $\hat{e}$ to every particle i pointing from the particle centre of $i-1$ to the centre of $i+1$. Then, we determine the angle between particle i and every neighbour j.

$$\theta_{ij} = \arccos(\hat{e}_i \cdot \hat{e}_j) \begin{cases} \leq 10^\circ & \text{"aligned"} \\ > 10^\circ & \text{"non-aligned"} \end{cases} . \quad (5)$$

Those particles whose number of "aligned" neighbours exceeds the threshold value (8 monomers in our study) are called crystalline particles. This threshold value is determined from the following analysis of the probability distribution of aligned neighbours in the bulk melt. We draw a probability distribution of aligned neighbours for an equilibrated melt and select the threshold number of

aligned neighbours to be the value where the probability reaches zero on the right-hand side of the bell shape curve of the probability distribution. This shows that no melt particles in the system have more aligned neighbours than this threshold value. Hence, if any particle has more aligned neighbours than this threshold value, it is a crystalline particle.

- Finally, the clusters of crystalline particles are identified using a standard clustering algorithm. The crystalline clusters in the system are identified by picking a random particle and checking if it is crystalline or not. If it is crystalline, we count it as the first particle of this cluster and examine its neighbours. If any neighbouring particle is also crystalline, it is counted as the second particle of the same cluster. Similarly, we move recursively from neighbour to neighbour to compute the cluster size. If a particle does not have any new crystalline neighbours, then we move to the next particle to identify the second cluster in the system and so on. At the end, all cluster sizes are compared and the largest cluster is identified.

We note here that, in our simulations whenever a nucleus that is significantly bigger than the critical nucleus (as define later) is seen, this always develops into a large crystalline structure.

C. Simulation details

We have performed molecular dynamics simulations of linear polymer chains to study nucleation under shear flow. The system consists of 300 chains of length 1000 monomers. We equilibrated the system at 550 K which is well above the equilibrium melting temperature (396.4 K) of polyethylene. This value of the melting temperature has been determined experimentally[76] and this force field reproduces the experimental melting temperature for short chain alkanes[42] and has been used for longer chains in previous studies[43]. We consider a system to be equilibrated once the chains have diffused a distance equal to their radius of gyration. Furthermore, we ran one very long equilibration trajectory of approximately three times this diffusion time. Our nucleation under flow results these two different lengths of equilibration are indistinguishable. We then run NPT simulations at temperatures at which we want to see nucleation and let it relax to the density that corresponds to 1 atm pressure. The system remained amorphous during these density relaxation simulations as the density relaxation at T_c, which was performed quiescently, took significantly less time than the flow-induced induction times. After getting these relaxed configurations, we fix the density again and raise the temperature to 550 K and let the melt relax at this temperature. We did this because we wanted to quench a fully relaxed system to the desired crystallisation temperature at the correct density. The densities of the metastable melt at 1 atm pressure and the corresponding temperatures are given in Table II.

All shear simulations have been performed under constant volume and constant temperature conditions. The shear flow has been generated using Lees Edwards boundary conditions[77] and the DPD thermostat[78] in the same way as Schilling and co-workers[72]. We took the friction coefficient for the thermostat to be 0.5 τ^{-1} and the cut-off radius to be $R_c = 1.3\sigma$, where $\tau = \sqrt{\frac{k_B T}{m\sigma^2}}$ and m is the mass of the bead, k_B is the Boltzmann constant, T is the temperature in Kelvin and σ is the size of the beads. We used the ESPResSo[79] molecular dynamics package for all simulations.

During nucleation simulations, we quenched the equilibrated configurations from 550 K to 380 K, 360 K and 340 K and applied the shear rate ($\dot{\gamma}$). We run simulations at three different temperatures and at three different values of the Rouse Weissenberg number ($W_{iR} = \dot{\gamma}\tau_R$). The integration timestep used in the simulations at 340 K was 0.0066τ. The factor 0.0066 was changed at different temperatures to keep the time step the same in seconds. We choose the flow timescale ($\dot{\gamma}$) to be slower than the Rouse time of an entanglement segment τ_e ($\dot{\gamma}\tau_e < 1$) so that, on the timescale of the flow, monomers have enough time to experience their surrounding constraints and entanglements have a strong influence on how the flow deforms the polymer chains. This is because any substantial strain ($\gamma > 1$) takes longer than the Rouse time of an entanglement segment and so the response to flow is always influenced by entanglements. In contrast, the timescale of a successful nucleation event is shorter than τ_e and so nucleation, itself, is not directly influence by entanglements. We define the timescale of a successful nucleation event as follows: we begin with a well formed crystal and run time backwards through the saved trajectory until the crystal is the critical nucleus size and call this τ_{crit}. We then continue to run time backwards, stopping when no monomers in the critical nucleus are crystalline and label this τ_{start}. This is the time just before the successful nucleation event begins. The time $\tau_{crit} - \tau_{start}$ measures the time from inception to stable nucleation for a single successful nucleation event. This observation is supported by quiescent nucleation simulations by Yi et. al[43]. They saw the same nucleation barrier for both entangled and unentangled chains, suggesting that nucleation, at least at this level of undercooling, is a local event occurring on a lengthscale shorter than the tube diameter. We used a total of approximately 2000 kCPU hours on the University of Nottingham and Midland Plus HPC facilities to carry out these simulations (equilibration, rheological characterisation and nucleation simulations).

III. RESULTS & DISCUSSION

A. Rouse relaxation time

Shear flow is expected to significantly change the nucleation rate above a shear rate that corresponds to a Rouse Weissenberg number of order 1. To determine the Weissenberg number, we must know the Rouse relaxation time of our system. There are many methods to determine the Rouse time from molecular dynamics simulations. Recently, Rutledge and co-workers[43] estimated the Rouse time from equilibrium molecular dynamics simulations by computing the end to end vector auto-correlation function. Cao and Likhtman[80] determined the Rouse time from equilibrium molecular dynamics simulations by calculating the stress relaxation auto-correlation function. We wish to calculate the Rouse relaxation time through stress simulation data to be consistent with rheological models and measurements. The tube model is widely used to study the rheology of polymers and it separates the molecular deformation into chain stretching and orientation. Chain stretching defines the Rouse time (τ_{R}) and chain orientation defines the reptation or terminal time ($\tau_{\mathrm{d}} \sim 3\mathrm{Z}\tau_{\mathrm{R}}$), where Z is the number of entanglements. We found that the usual method to extract the relaxation time based on equilibrium simulations of the stress relaxation auto-correlation function was prohibitively expensive, requiring a simulation of $\sim 10\ \tau_{\mathrm{d}}$ to get good statistics for the terminal time[81]. Therefore, we devised a new way to extract the Rouse relaxation time based on non-equilibrium molecular dynamics simulations which requires a simulation of length $\sim 4\ \tau_{\mathrm{R}}$. We describe this method in detail here.

In this method, we run non-equilibrium molecular dynamics simulations at 450 K to compute the transient shear viscosity, which we show in FIG. 1. We run simulations at shear rates of $\dot{\gamma} = 0.000002\tau^{-1}$ and $\dot{\gamma} = 0.0001\tau^{-1}$. In this figure, the simulation data are shown with symbols and the GLaMM model[82] fitting is represented with lines. In the GLaMM model, three input parameters are used to obtain the best fit. These parameters are the entanglement modulus ($\mathrm{G_e}$), the Rouse relaxation time of an entanglement segment (τ_{e}) and the number of monomers per entanglement ($\mathrm{N_e}$). We used the standard value of 0.1 for the constraint release parameter (c_ν). The Rouse time can be calculated using the relation $\tau_{\mathrm{R}} = \tau_{\mathrm{e}}\mathrm{Z}^2$, where $\mathrm{Z} = \mathrm{N}/\mathrm{N_e}$ and N is the number of monomers in a chain. We have also computed N_e using the Z1 code[83–86], which uses a primitive path analysis approach to estimate the number of chain entanglements. We find the entanglement length to be 72 monomers ($\mathrm{Z} \sim 13.84$), which is in very close agreement with the rheologically determined value.

Once we have the Rouse time at a single temperature, we can then estimate the Rouse time at all other temperatures by running short equilibrium molecular dynamics trajectories at the desired temperatures. From these trajectories, we calculate the stress relaxation modulus (G(t)) and then we shift all curves to the reference temperature curve based on the time-temperature superposition (TTS) concept[87,88] using the same approach as widely used for experimental data[88–94]. We apply TTS to G(t) in the following way:

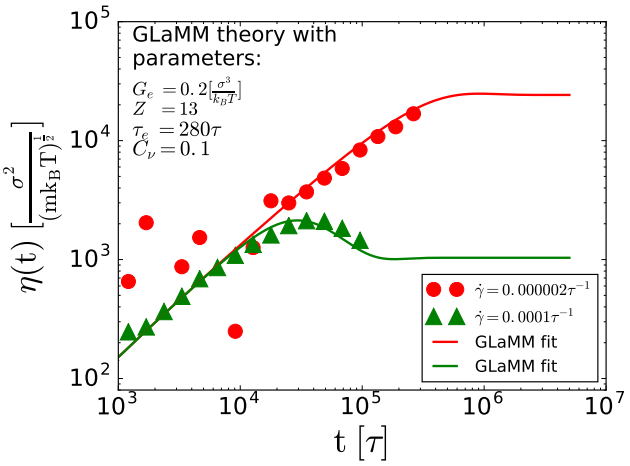

FIG. 1: Shear viscosity from non-equilibrium molecular dynamics simulations. Simulation data is represented with symbols and the GLaMM model[82], as fitted to the simulation data, is shown with lines.

$$G(t, T_0) = b_T^{-1}(T) G(t/a_T, T), \tag{6}$$

where $\mathrm{T_0}$ is the reference temperature ($\mathrm{T_0} = 450\mathrm{K}$ in this work), t is the time, T is the temperature from which G(t) is to be shifted and $\mathrm{b_T}$ and $\mathrm{a_T}$ are the vertical and horizontal shift factors respectively. The value of the vertical shift $\mathrm{b_T}$ is specified by the densities:

$$b_T = \frac{\rho(T) T}{\rho(T_0) T_0}, \tag{7}$$

where $\mathrm{T_0}$ and $\rho(\mathrm{T_0})$ are the temperature and density to which the data is shifted. All densities were determined by NPT simulations and are in Table II.

The temperature dependence of the horizontal shift factor a_T can be expressed using the Arrhenius equation, given as follows:

$$a_T = \exp\left[\frac{E_a}{R}\left(\frac{1}{T} - \frac{1}{T_0}\right)\right], \tag{8}$$

where $\mathrm{E_a}$ is the activation energy of flow and R is the universal gas constant. This relation gives a good fit of the data in the plateau and terminal zones for temper-

atures well above the glass transition temperature T_g, which has been reported as 223.04 ± 0.22K[43] for this force field. The temperature dependence of the horizontal shift factor a_T for a temperature range between T_g and $T_g + 100$ K can be expressed by the Williams-Landel-Ferry (WLF) equation[91,95]:

$$\log(a_T) = \frac{-c_1(T - T_0)}{c_2 + (T - T_0)}, \tag{9}$$

where c_1 and c_2 are material parameters. We determined the value of the horizontal shift factor a_T by manually shifting the G(t) curves to the G(t) curve for the reference temperature $T_0 = 450$K, which generated a master curve for G(t).

The Rouse time (τ_R^T) can then be estimated for different temperatures from the horizontal shift factor (a_T) and the Rouse time at the reference temperature ($\tau_R^{T_0}$) as follows:

$$\tau_R^T = \tau_R^{T_0} a_T. \tag{10}$$

In FIG. 2(a), we show simulation data for the stress relaxation modulus (G(t)) at different temperatures for a short period of time. We select the curves from the highlighted region because the curves are statistically rich in this region when compared to the later time curves. We already have the Rouse time at 450 K, which we have calculated from non-equilibrium simulations and the GLaMM model fit. Now, we have to shift the curves vertically using EQU 7 and then move the curves horizontally to superpose the curves on the reference curve (450 K). In FIG. 2(b), we show the shifted and superposed curves from different temperatures and the reference curve at 450 K. From here we obtain different values of the horizontal shift factor (a_T) for different temperatures which we show in FIG. 2(c) and in tabulated form in Table II. We also show fits to the data of the horizontal shift factors (a_T) using the Arrhenius equation (EQU 8) and the WLF equation (EQU 9) with solid black and blue lines respectively. The value of the activation energy (E_a) was found to be 31 KJ/mole for the best fit. This value is very close to the experimentally reported value (26.77 KJ/mole)[96] and numerically reported value (21.46±3.30KJ/mole)[43]. A detailed discussion of the variation of the activation energy with different measurement techniques can be found in these works[93,94]. The Arrhenius equation fits well for temperatures well above the glass transition temperature, while the WLF equation fits better for the whole range of temperatures with material constants c1 = 2.05 and c2 = 300K.

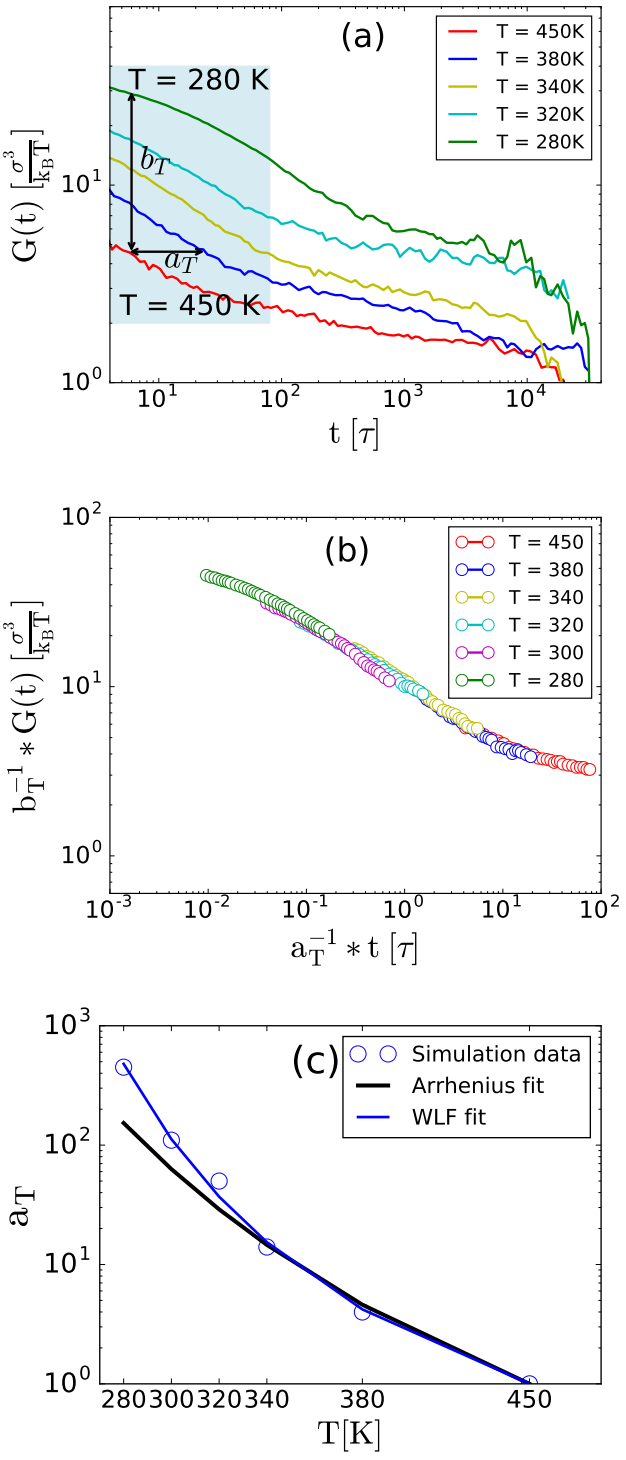

FIG. 2: (a) The stress-relaxation modulus at different temperatures against time. We selected the part of the curves which are highlighted in light blue for the time-temperature superposition process. (b) The master curve for the stress-relaxation modulus is generated by shifting all curves to a reference temperature curve. (c) The horizontal shift against temperature including simulation data (circles) and fitting to this data (solid lines).

TABLE II: The density and horizontal and vertical shifts for our C1000 melt simulations of polyethylene at 1 atmospheric pressure.

Temperature $[K]$	Density $[g/cm^3]$	b_T	a_T	τ_R[ns]
450	0.836	1	1	38.8
380	0.867	0.875	4	155.2
360	0.876	0.838	7.56	293.4
340	0.884	0.798	14	543.2
320	0.893	0.759	50	1940
300	0.901	0.718	110	4268
280	0.9098	0.676	450	17460

B. Crystal nucleation

We perform molecular dynamics simulations at three different temperatures for three different values of the Rouse Weissenberg number to calculate the induction time (τ^*). In nucleation studies, estimation of the induction time is an important step particularly from molecular dynamics simulations. This involves the appropriate selection of an order parameter to identify the largest crystal cluster in the melt from the trajectories and then selection of a method to estimate the induction time. We use the crystallinity order parameter that we described in section II B and we use a mean first passage time (MFPT) approach[97], which is based on classical nucleation theory, to estimate the induction time. Mean first passage time analysis is performed on the evolution of the largest cluster in the system to define the average time of the first appearance of a cluster with size n_{max}:

$$\tau(n_{max}) = \frac{1}{M}\sum_{i=1}^{M}\tau_{n_{max}}^{(i)}, \qquad (11)$$

where M is the total number of trajectories and $\tau_{n_{max}}^{(i)}$ is the time when a cluster with size n_{max} first appears. As nucleation is followed by fast cluster growth, $\tau(n_{max})$ has a sigmoidal shape and can be fitted by the equation:

$$\tau(n_{max}) = 0.5\tau^*[1 + \mathrm{erf}(Z\sqrt{\pi}(n_{max} - n^*))], \qquad (12)$$

where τ^* is the induction time, n* is the critical nucleus size, Z is the Zeldovich factor and the error function is $\mathrm{erf} = \frac{2}{\sqrt{\pi}}\int_0^x e^{-x^2}dx$. This mean first passage time has been successfully used for this purpose in many recent studies[41–43,45,72].

It is a common perception that flow enhances the nucleation rates by inducing local orientation of polymer chains. Under flow, temperature plays an important role in two ways. Firstly, at higher temperatures, the relaxation times are shorter, meaning lower orientation.

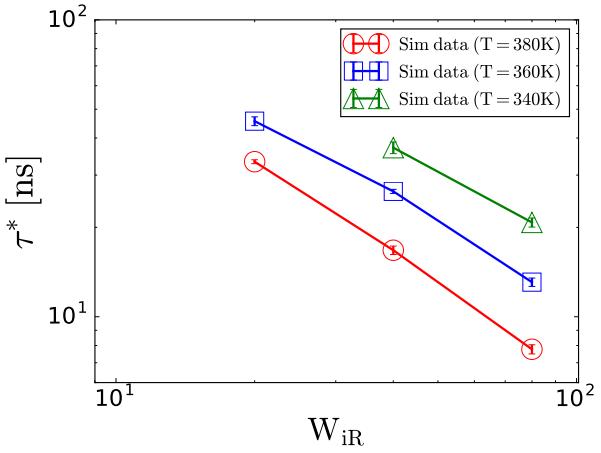

FIG. 3: Simulated induction time as a function of the Rouse Weissenberg number.

Secondly, temperature affects the quiescent crystallisation kinetics. Therefore, the coupled effect of flow and temperature needs to be addressed. The effects of flow and temperature on the induction time have been studied experimentally[15,98] and theoretically[15]. These studies show that the effect of flow on the induction time can be divided into two distinct regions. For low Weissenberg numbers there is no effect of shear flow on the induction time, while for high Weissenberg numbers, the induction time decreases as a power law in shear rate. Furthermore, the slope of the curves in the second region ($W_{iR} \geq 1$) at higher temperatures is greater than the slope at lower temperatures. This means that at very high shear rates, the induction times for different temperatures start to converge. We show experimental observations of these effects in FIG. 4(b), which has been taken from the literature[15]. This same effect has been seen in the Graham and Olmsted[35,36] kinetic Monte Carlo model. In this model, the increased sensitivity to flow occurs because higher undercooling produces larger critical nuclei, which can incorporate more stretched chain segments[99].

We computed the induction time, as show in FIG. 3. This figure shows that the induction times are lower at higher temperatures for the same Rouse Weissenberg number (W_{iR}) which is contrary to the observations made in experiments[15,98,100,101] and theory[15,34]. However, when we incorporated the monomer friction by dividing the induction times by Rouse times (τ_R) (see FIG. 4(a)), we too observe the same trend as reported in the previously published literature from experiments and Monte Carlo simulations, namely a more pronounced effect of flow at higher temperatures. We can explain need to divide the induction time by the Rouse time using classical nucleation theory. According to classical nucleation theory, the nucleation rate depends on the product of a kinetic factor and the Boltzmann factor of the nu-

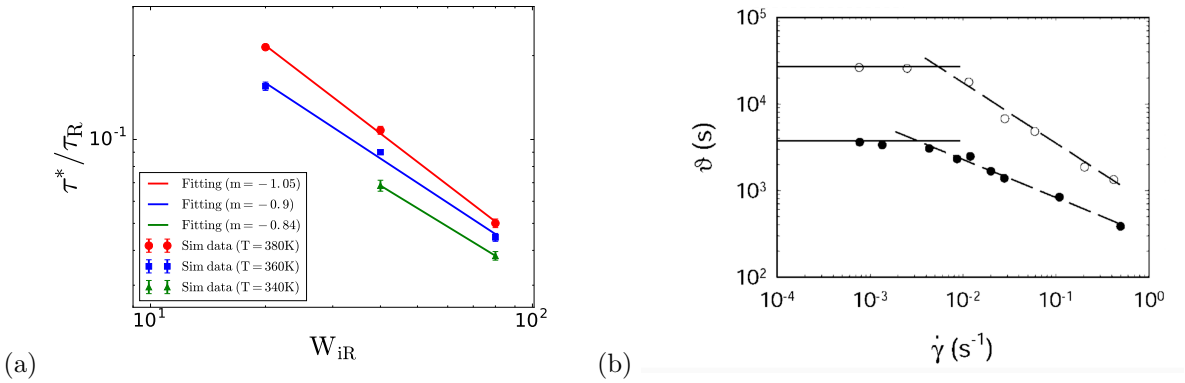

FIG. 4: Simulated induction time against the Rouse Weissenberg number with the induction time normalised by the Rouse time (a). Experimentally measured[15] induction time, ϑ, against shear rate (b). Part (b) reprinted from ref[15], Copyright (2004) with the permission of Elsevier.

cleation barrier height. The former is proportional to the monomer friction. In experiments, usually the degree of supercooling is very low and experiments are run at temperatures that are far from T_g and have only a few degrees difference. Therefore, this monomer friction factor does not change significantly between these temperature. In contrast, in our molecular dynamics simulations, the kinetic prefactor changes more strongly between the different temperatures. This is because the degree of supercooling is relatively large so we are much closer to T_g and the differences between the temperatures at which simulations are run are high (20K difference in our case). Therefore, we divide induction time by the Rouse time in MD simulations to correct for the strong dependence of the induction time on the monomer friction. We fitted power laws to the data from each temperature to obtain the exponent with shear rate, as shown in FIG 4(a). The window of induction times we were able to access in MD was too limited to observe the cross-over to quiescent behaviour as in experiments. Longer simulations, perhaps utilising a fast nucleation algorithm[102,103], will be needed to see this effect.

Our induction time data can also be converted to an induction strain γ_I, computed by multiplying the induction time by the shear rate. The induction strain can be considered as the level of shear strain required to start crystallisation. We show the induction shear strain against the Rouse Weissenberg number from our simulations in FIG. 5(a). As expected, the induction strain increases with temperature. However, the dependence on shear rate shows some counter-intuitive behaviour. At the highest temperature γ_I decreases with shear rate, at the intermediate temperature γ_I is almost constant and at the lowest temperature γ_I increases with shear rate. Nevertheless, these qualitative features have been seen in experiments[100] as shown in FIG. 5(b). In section IV, we offer an interpretation of this observation, by considering the degree of chain stretch at nucleation.

In order to determine the spread of the induction time and its corresponding stress and strain values, we show histograms of the observed induction times and stress (σ_{xy}) with red bars and blue lines respectively in FIG. 6 at two different temperatures and different values of the Rouse Weissenberg number (W_{iR}) (Further simulation data for three different temperatures and at two different values of the Rouse Weissenberg number can be seen in appendix A). The histograms of the observed induction times and stress have been computed from MD simulations and the GLaMM model[82], respectively. For the GLaMM model, we used the same parameters that we obtained during relaxation time calculations. The induction times are narrowly distributed, with all nucleation events occurring within a narrow time span. The stress curve shows that all nucleation events occur in transient conditions. The shear strain is another important factor in flow induced nucleation. The strain (γ) value at nucleation ranges between 1.63 and 3.34 (appendix A).

IV. INTERPRETATION OF NUCLEATION DATA

The value of γ_I represents the macroscopic strain at the time of nucleation. However, the microscopic strain on the chain level is likely to be different due to chain relaxation. The microscopic strain can be observed via the chain stretch ratio, defined as the fractional increase in the tube contour length ($Z^*(t)/Z$) as computed from the GLaMM model[82]. In order to compute the stretch from the GLaMM model, we used the parameters that we extracted in the relaxation time calculations by fitting the GLaMM model to our MD simulations. We plot the chain stretch, from the GLaMM model, at the induction time, from MD simulation, in FIG. 7. This induction stretch, λ_I, shows three key features: λ_I increases with increasing temperature; λ_I increases weakly with flow rate; and the increase in λ_I with flow rate is steeper at

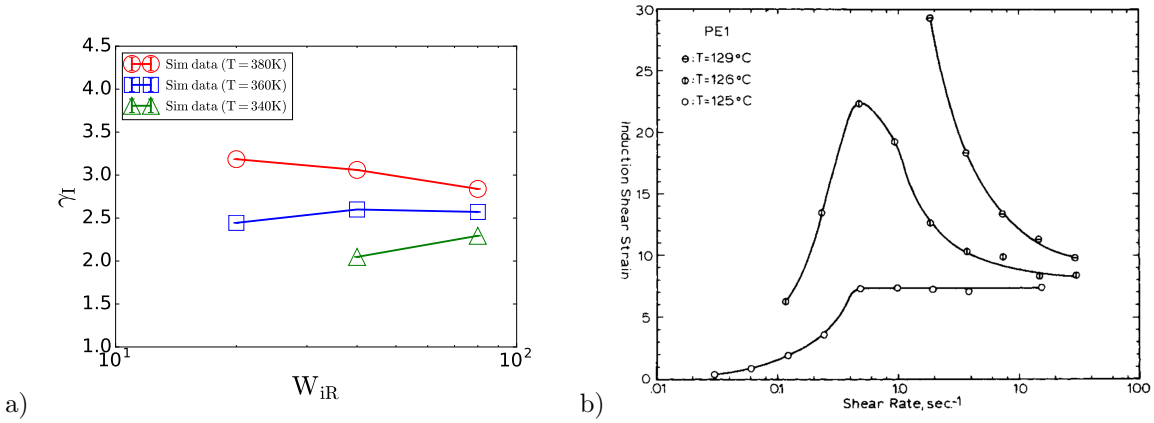

FIG. 5: Shear strain required to induce crystallisation in linear polymer chains: (a) simulations from this work and (b) experiments from[100] (b). Part (b) reprinted from ref[100], Copyright (2004) with the permission of John Wiley and Sons.

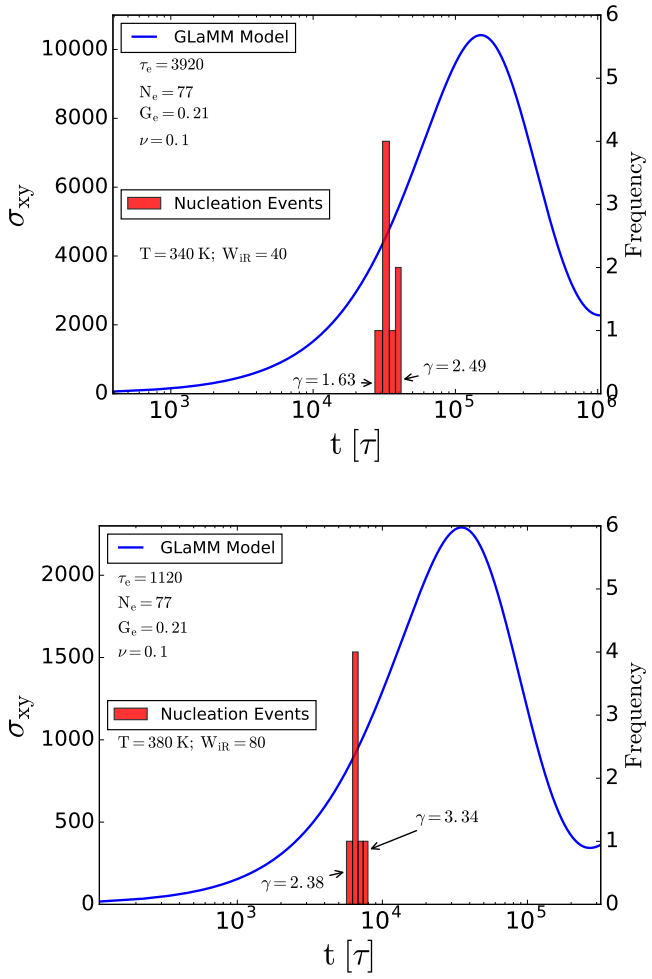

FIG. 6: The stress and frequency of induction time against the time at 340K (Top) and at 380K (Bottom).

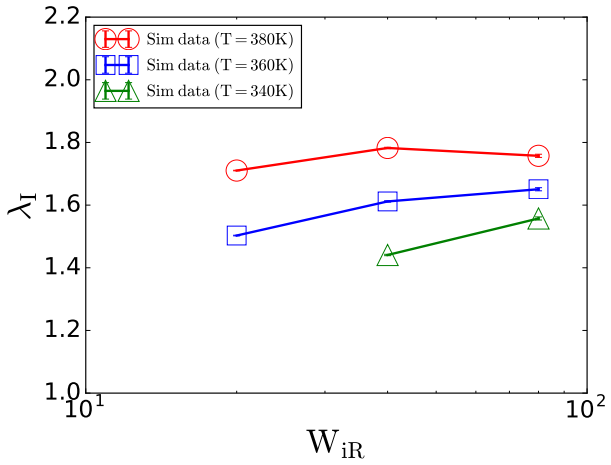

FIG. 7: Stretch required to induce crystallisation in our C1000 simulations.

lower temperatures. We interpret these data by postulating that the induction time comprises of two contributions: the time required to achieve sufficient stretch that nucleation becomes highly likely, τ_{λ^*}, minus the contributions from the nuclei that manage to cross the barrier before λ^* is reached, τ_{early}. This explains the three key features of FIG. 7: λ_I increases with temperature because the increased quiescent nucleation barrier requires greater stretch to sufficiently lower the barrier (i.e. λ^* increases with temperature); λ_I increases with flow rate because, at slower flow rates, the longer time to reach λ^* permits more early nucleation events (i.e. τ_{early} decreases with increasing flow rate); and the lower barriers at lower temperatures allow more nucleation prior to λ^*, giving a larger role for τ_{early}. Indeed FIG. 7 shows that λ_I is virtually constant at 380K, suggesting an insignificant effect of τ_{early}, whereas somewhat steeper increases

in λ_I are seen at lower temperatures. This interpretation explains the counter-intuitive results for the variation in induction strain with shear rate in figure 5 as a combination of the strain required to obtain the critical chain stretch and the probability of early nucleation events before this critical stretch is reached.

We show histograms of the observed induction times (computed from MD simulations) and stretch (computed from the GLaMM model[82]) with red bars and blue lines respectively in FIG. 8. The stretch curve shows that all nucleation events occur in transient conditions and the stretch value is smaller than the steady stretch value. Further data for the stretch and induction times are shown in appendix B. From figures (FIG. 6 and FIG. 8), we can deduce that nucleation happens early in the transient, when the molecular stretch is significantly below both the transient maximum and steady state value. This suggests that at this under-cooling, the flow very readily induces nucleation even at fairly modest molecular deformation. This illustrates the type of information that is difficult to extract from experiments but can be obtained from MD.

V. CONCLUSIONS

We carried out united-atom molecular dynamics simulations to characterise the nucleation behaviour of entangled linear polymers under shear flow. We studied well-entangled C1000 chains, for which we determined the Rouse relaxation time by fitting a tube model to shear stress data from simulations of non-linear start-up shear. We characterised the temperature dependence of this timescale via time-temperature superposition. From our crystallisation simulations we computed the induction time at a range of Weissenberg numbers and for several temperatures. We found a more pronounced effect of flow rate on the induction times at higher temperatures. Also we observed a weak dependence of the induction strain on shear rate, with the slope of this dependence decreasing and changing sign with increased temperature. Both of these effects are also seen experimentally and our results provide a direct confirmation that these phenomena can be predicted from molecular dynamics simulations. We presented results for the distribution of induction times, compared to the shear stress transient predicted by the GLaMM model. For a given temperature and shear rate the distribution of induction times is quite narrow. Furthermore, all nucleation events occur early in the start-up flow, before the shear stress overshoot.

By using the microscopic chain stretch at the time of nucleation, as computed by the GLaMM model, we are able to explain the counter-intuitive results for the variation of induction strain with shear rate in figure 5. We postulated that the induction strain is a combination of the strain required to obtain the critical chain stretch and the probability of early nucleation events before this critical stretch. This qualitatively explains all of our induction time results and suggests explanations for several experimentally observed phenomena.

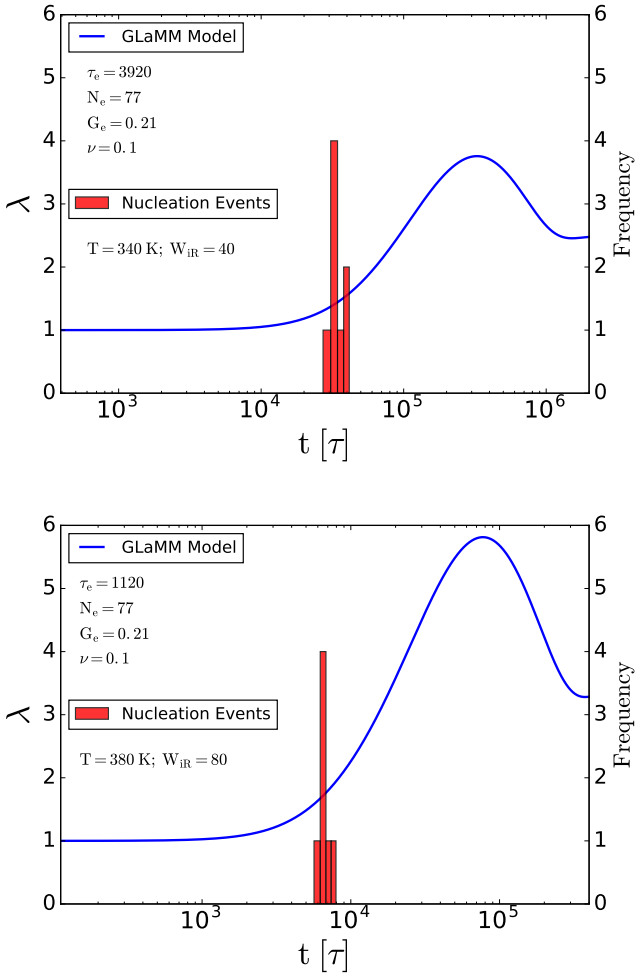

FIG. 8: The stretch and induction time histograms against the time at 340K (Top) and at 380K (Bottom).

ACKNOWLEDGMENTS

We thank Greg Rutledge, Ron Larson and Ralph Colby for useful discussions about polymer FIC. We gratefully acknowledge funding from the EPSRC (grant no. EP/P005403/1), access to the University of Nottingham High Performance Computing Facility and the use of Athena at HPC Midlands+, which was funded by the EPSRC on grant EP/P020232/1, as part of the HPC Midlands+ consortium.

Appendix A: The stress transient and the induction time histograms

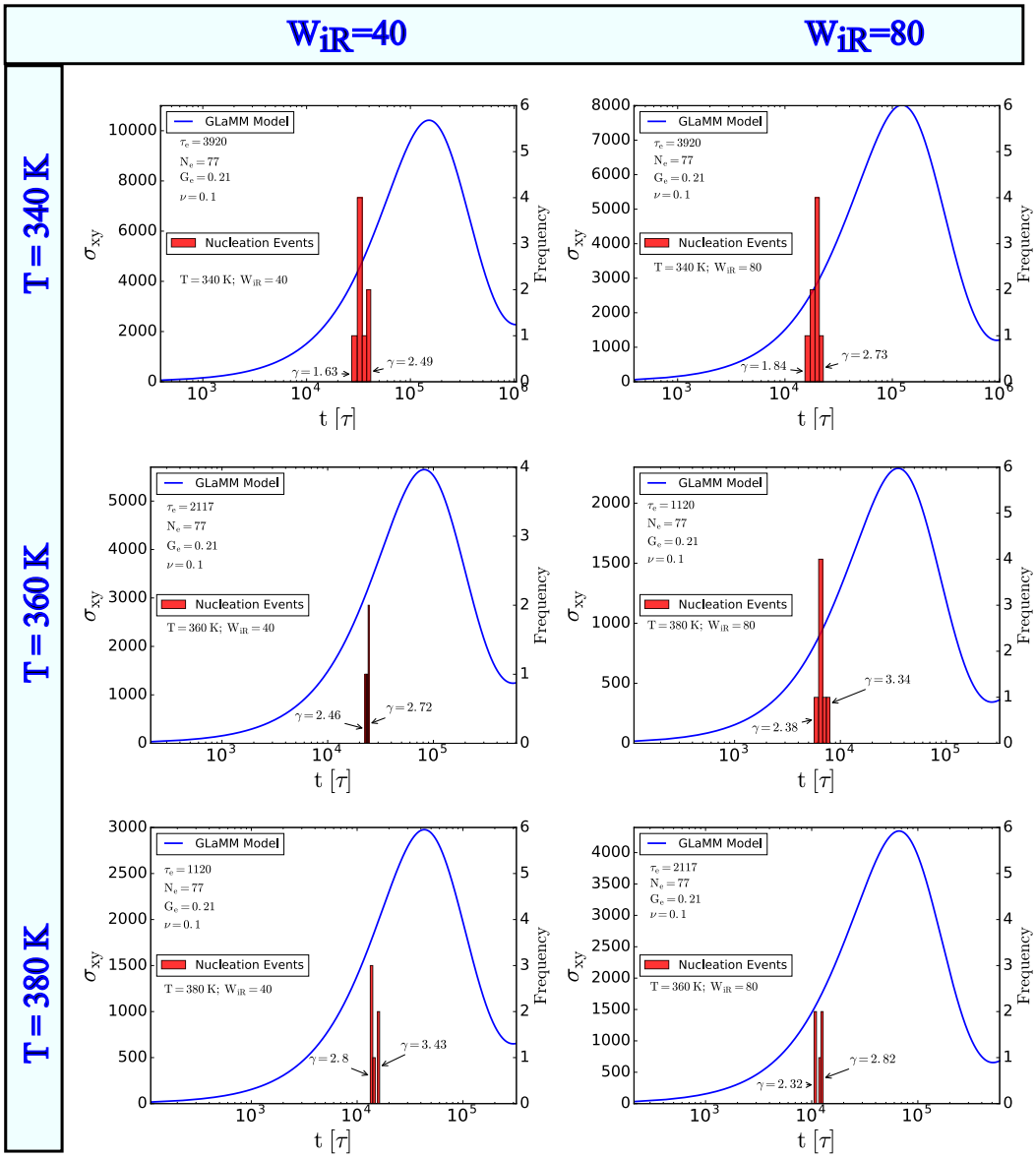

FIG. 9: The stress and induction time histograms against the time.

Appendix B: The stretch transient and induction time histograms

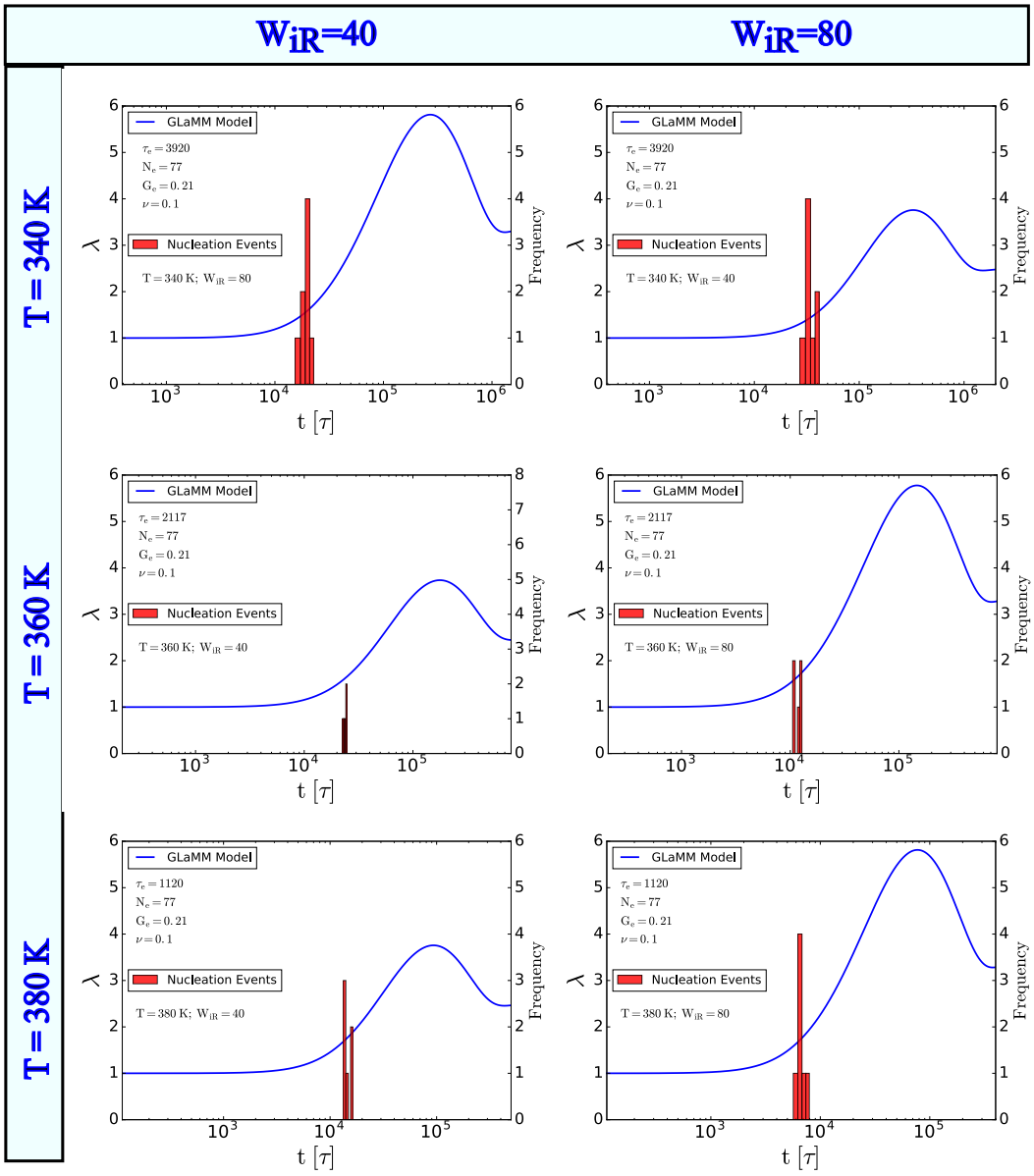

FIG. 10: The chain stretch and induction time histograms against the time.

Appendix C: Nucleation details

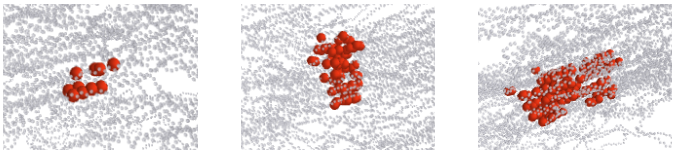

FIG. 11: The evolution of the critical nucleus from a trajectory, when it first appears with a cluster size of 10 monomers (left), with a size of 61 monomers (middle) and with 140 monomers (right). The critical nucleus size is approximately 70 monomers.

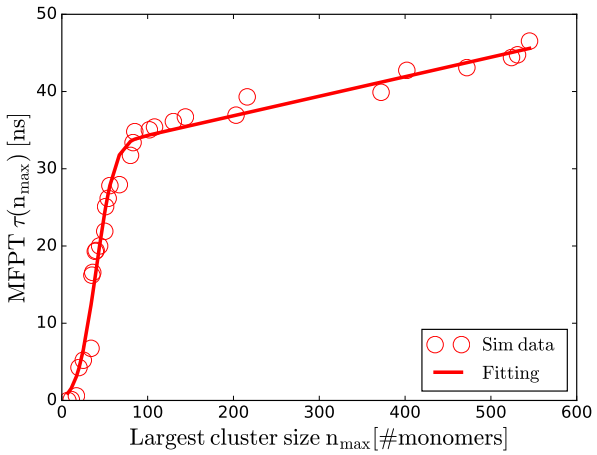

FIG. 12: The mean first passage time curve from simulation data is shown with circles and the fitting of equation 12 to simulation data with red line.

[1]M. Imai, K. Kaji, and T. Kanaya. Structural formation of poly(ethylene terephthalate) during the induction period of crystallization. 3. evolution of density fluctuations to lamellar crystal. *Macromolecules*, 27(24):7103–7108, 1994.

[2]M. Imai, K. Kaji, T. Kanaya, and Y. Sakai. Ordering process in the induction period of crystallization of poly(ethylene terephthalate). *Phys. Rev. B*, 52:12696–12704, 1995.

[3]T. A. Ezquerra, E. López-Cabarcos, B. S. Hsiao, and F. J. Baltà-Calleja. Precursors of crystallization via density fluctuations in stiff-chain polymers. *Phys. Rev. E*, 54:989–992, Jul 1996.

[4]A. Keller, M. Hikosaka, S. Rastogi, A. Toda, P.J. Barham, and G. Goldbeck-Wood. An approach to the formation and growth of new phases with application to polymer crystallization: effect of finite size, metastability, and ostwald's rule of stages. *Journal of Materials Science*, 29(10):2579–2604, 1994.

[5]M. Imai, K. Mori, T. Mizukami, K. Kaji, and Kanaya T. Structural formation of poly(ethylene terephthalate) during the induction period of crystallization:1. ordered structure appearing before crystal nucleation. *Polymer*, 33:4451, 1992.

[6]G. Strobl. From the melt via mesomorphic and granular crystalline layers to lamellar crystallites: A major route followed in polymer crystallization? *The European Physical Journal E*, 3(2):165–183, 2000.

[7]G. Strobl. A thermodynamic multiphase scheme treating polymer crystallization and melting. *The European Physical Journal E*, 18(3):295–309, 2005.

[8]Gert Strobl. Crystallization and melting of bulk polymers: New observations, conclusions and a thermodynamic scheme. *Progress in Polymer Science*, 31:398442, 2006.

[9]T. Y. Cho G. Strobl. Growth kinetics of polymer crystals in bulk. *Eur. Phys. J. E*, 23:55, 2007.

[10]Gert Strobl. ¡i¿colloquium¡/i¿: Laws controlling crystallization and melting in bulk polymers. *Rev. Mod. Phys.*, 81:1287–1300, Sep 2009.

[11]R.H. Somani, L. Yang, I. Sics, B.S. Hsiao, N.V. Pogodina, H.H. Winter, P. Agarwal, H. Fruitwala, and A. Tsou. Orientation-induced crystallization in isotactic polypropylene melt by shear deformation. *Macromolecular Symposia*, 185(1):105–117, 2002.

[12]Rajesh H. Somani, Ling Yang, and Benjamin S. Hsiao. Precursors of primary nucleation induced by flow in isotactic polypropylene. *Physica A: Statistical Mechanics and its Applications*, 304(12):145 – 157, 2002. Scattering Studies of Mesoscopic Scale Structure and Dynamics in Soft Matter.

[13]Ferass M Abuzaina, Benjamin D Fitz, Saa Andjeli, and Dennis D Jamiolkowski. Time resolved study of shear-induced crystallization of poly(p-dioxanone) polymers under low-shear, nucleation-enhancing shear conditions by small angle light scattering and optical microscopy. *Polymer*, 43(17):4699 – 4708, 2002.

[14]G. Floudas D. Lellinger and I. Alig. Shear induced crystallization in poly(ϵ-caprolactone): effect of shear rate. *Polymer*, 44(19):5759 – 5769, 2003.

[15]Salvatore Coppola, Luigi Balzano, Emilia Gioffredi, Pier Luca Maffettone, and Nino Grizzuti. Effects of the degree of undercooling on flow induced crystallization in polymer melts. *Polymer*, 45(10):3249 – 3256, 2004.

[16]Aadil Elmoumni and H.Henning Winter. Large strain requirements for shear-induced crystallization of isotactic polypropylene. *Rheologica Acta*, 45(6):793–801, 2006.

[17]S. Acierno and N. Grizzuti. Flow-induced crystallization of polymer: theory and experiments. *International Journal of Material Forming*, 1(1):583–586, 2008.

[18]Ri-Chao Zhang, Ai Lu, and Zhong-Bin Xu. Effect of molecular weight on crystallization of semirigid poly(phenylene sulfide) under shear flow. *Journal of Applied Polymer Science*, 124(2):1562–1569, 2012.

[19]I. Coccorullo, R. Pantani, and G. Titomanlio. Spherulitic nucleation and growth rates in an ipp under continuous shear flow. *Macromolecules*, 41(23):9214–9223, 2008.

[20]Shuichi Kimata, Takashi Sakurai, Yoshinobu Nozue, Tatsuya Kasahara, Noboru Yamaguchi, Takeshi Karino, Mitsuhiro Shibayama, and Julia A. Kornfield. Molecular basis of the shish-kebab morphology in polymer crystallization. *Science*, 316(5827):1014–1017, 2007.

[21]Benjamin S. Hsiao, Ling Yang, Rajesh H. Somani, Carlos A. Avila-Orta, and Lei Zhu. Unexpected shish-kebab structure in a sheared polyethylene melt. *Phys. Rev. Lett.*, 94:117802, Mar 2005.

[22]Luigi Balzano, Nileshkumar Kukalyekar, Sanjay Rastogi, Gerrit W. M. Peters, and John C. Chadwick. Crystallization and dissolution of flow-induced precursors. *Phys. Rev. Lett.*, 100:048302, Feb 2008.

[23]Motohiro Seki, Derek W. Thurman, James P. Oberhauser, and Julia A. Kornfield. Shear-mediated crystallization of isotactic polypropylene: the role of long chainlong chain overlap. *Macromolecules*, 35(7):2583–2594, 2002.

[24]Frederico JMF Custódio, Rudi JA Steenbakkers, Patrick D Anderson, Gerrit WM Peters, and Han EH Meijer. Model development and validation of crystallization behavior in injection molding prototype flows. *Macromolecular Theory and Simulations*, 18(9):469–494, 2009.

[25]Jan van Meerveld, Markus Htter, and Gerrit W.M. Peters. Continuum model for the simulation of fiber spinning, with quiescent and flow-induced crystallization. *Journal of Non-Newtonian Fluid Mechanics*, 150(2):177 – 195, 2008.

[26]Hans Zuidema, Gerrit W. M. Peters, and Han E. H. Meijer. Development and validation of a recoverable strain-based model for flow-induced crystallization of polymers. *Macromolecular Theory and Simulations*, 10(5):447–460, 2001.

[27]S.F. Edwards M. Doi. *The Theory of Polymer Dynamics*. Oxford University Press, 1986.

[28]Takayuki Shimada, Masao Doi, and Koji Okano. Concentration fluctuation of stiff polymers. iii. spinodal decomposition. *The Journal of Chemical Physics*, 88(11):7181–7186, 1988.

[29]P. D. Olmsted, W. C. K. Poon, T. C. B. McLeish, N. J.Terrill, and A. J. Ryan. Spinodal-assisted crystallization in polymer melts. *Physical Review Letters*, 81:373–376, 1998.

[30]Bing Miao Hongge Tan and Dadong Yan. Conformation-assisted fluctuation of density and kinetics of nucleation in polymer melts. *The Journal of Chemical Physics*, 119(5):2886–2891, 2003.

[31]K. Kaji. *Handbook of Thermoplastic Polyesters: Homopolymers, Copolymers, Blends, and Composites*, chapter Structure Formation in PET during the Induction Period of Crystallization, pages 225–251. Wiley-VCH Verlag GmbH & Co. KGaA, 2005.

[32]Claire McIlroy and Richard S Graham. Modelling flow-enhanced crystallisation during fused filament fabrication of semi-crystalline polymer melts. *Additive Manufacturing*, 24:323, 2018.

[33]Jimmy Baert and Peter Van Puyvelde. Density fluctuations during the early stages of polymer crystallization: An overview. *Macromolecular Materials and Engineering*, 293(4):255–273, 2008.

[34]Chunlei Ruan. Kinetics and morphology of flow induced polymer crystallization in 3d shear flow investigated by Monte Carlo simulation. *Crystals*, 7(2), 2017.

[35]Richard S. Graham and Peter D. Olmsted. Coarse-grained simulations of flow-induced nucleation in semicrystalline polymers. *Phys. Rev. Lett.*, 103:115702, Sep 2009.

[36]Richard S Graham and Peter D Olmsted. Kinetic monte carlo simulations of flow-induced nucleation in polymer melts. *Faraday discussions*, 144:71–92, 2010.

[37]K. Esselink, P. A. J. Hilbers, and B. W. H. van Beest. Molecular dynamics study of nucleation and melting of n-alkanes. *The Journal of Chemical Physics*, 101(10):9033–9041, 1994.

[38]Hisao Takeuchi. Structure formation during the crystallization induction period of a short chain-molecule system: A molecular dynamics study. *The Journal of Chemical Physics*, 109(13):5614–5621, 1998.

[39]Susumu Fujiwara and Tetsuya Sato. Molecular dynamics simulation of structural formation of short polymer chains. *Phys. Rev. Lett.*, 80:991–994, Feb 1998.

[40]Susumu Fujiwara and Tetsuya Sato. Molecular dynamics simulation of structure formation of short chain molecules. *The Journal of Chemical Physics*, 110(19):9757–9764, 1999.

[41]Peng Yi and Gregory C. Rutledge. Molecular simulation of crystal nucleation in n-octane melts. *The Journal of Chemical Physics*, 131:1–12, 2009.

[42]Peng Yi and Gregory C. Rutledge. Molecular simulation of bundle-like crystal nucleation from n-eicosane melts. *The Journal of Chemical Physics*, 135:11, 2011.

[43]Peng Yi, C Rebecca Locker, and Gregory C Rutledge. Molecular Dynamics Simulation of Homogeneous Crystal Nucleation in Polyethylene. *Macromolecules*, 46(11):4723–4733, 2013.

[44]Hasan Zerze, Jeetain Mittal, and Anthony J. McHugh. Ab initio crystallization of alkanes: Structure and kinetics of nuclei formation. *Macromolecules*, 46(22):9151–9157, 2013.

[45]Muhammad Anwar, Francesco Turci, and Tanja Schilling. Crystallization mechanism in melts of short n-alkane chains. *The Journal of Chemical Physics*, 139(21):–, 2013.

[46]Takashi Yamamoto. Molecular dynamics of polymer crystallization revisited: Crystallization from the melt and the glass in longer polyethylene. *The Journal of Chemical Physics*, 139(5):–, 2013.

[47]Takashi Yamamoto. Molecular dynamics simulations of polymer crystallization in highly supercooled melt: Primary nucleation and cold crystallization. *The Journal of Chemical Physics*, 133(3):–, 2010.

[48]Takashi Yamamoto. Molecular dynamics simulations of steady-state crystal growth and homogeneous nucleation in polyethylene-like polymer. *The Journal of Chemical Physics*, 129(18):–, 2008.

[49]Takashi Yamamoto. Molecular dynamics modeling of polymer crystallization from the melt. *Polymer*, 45(4):1357 – 1364, 2004.

[50]Takashi Yamamoto. Molecular-dynamics simulation of polymer ordering. i. crystallization from vapor phase. *The Journal of Chemical Physics*, 109(11):4638–4645, 1998.

[51]Chuanfu Luo and Jens-Uwe Sommer. Growth pathway and precursor states in single lamellar crystallization: MD simulations. *Macromolecules*, 44(6):1523–1529, 2011.

[52]Chuanfu Luo and Jens-Uwe Sommer. Coexistence of melting and growth during heating of a semicrystalline polymer. *Phys. Rev. Lett.*, 102:147801, Apr 2009.

[53]P. Welch and M. Muthukumar. Molecular mechanisms of polymer crystallization from solution. *Phys. Rev. Lett.*, 87:218302, Nov 2001.

[54]Hendrik Meyer and Florian Mller-Plathe. Formation of chain-folded structures in supercooled polymer melts. *The Journal of Chemical Physics*, 115(17):7807–7810, 2001.

[55]Jens-Uwe Sommer and Gnter Reiter. Polymer crystallization in quasi-two dimensions. ii. kinetic models and computer simulations. *The Journal of Chemical Physics*, 112(9):4384–4393, 2000.

[56]N. Waheed, M. S. Lavine, and G. C. Rutledge. Molecular simulation of crystal growth in n-eicosane. *The Journal of Chemical Physics*, 116(5):2301–2309, 2002.

[57]M. Muthukumar. *Modeling Polymer Crystallization*, volume 191 of *Advances in Polymer Science*, pages 241–274. Springer Berlin Heidelberg, 2005.

[58]M Muthukumar. Molecular modeling of nucleation in polymers. *Phil. Trans. Roy. Soc.*, A361:539–556, 2003.

[59]M. Muthukumar. Commentary on theories of polymer crystallization. *The European Physical Journal E*, 3(2):199–202, 2000.

[60]Chuanfu Luo and Jens-Uwe Sommer. Frozen topology: Entanglements control nucleation and crystallization in polymers. *Phys. Rev. Lett.*, 112:195702, May 2014.

[61]Akira Koyama, Takashi Yamamoto, Koji Fukao, and Yoshihisa Miyamoto. Molecular dynamics simulation of polymer crystallization from an oriented amorphous state. *Phys. Rev. E*, 65:050801, May 2002.

[62]Akira Koyama, Takashi Yamamoto, Koji Fukao, and Yoshihisa Miyamoto. Molecular dynamics studies on polymer crystallization from a stretched amorphous state. *Journal of Macromolecular Science, Part B*, 42(3-4):821–831, 2003.

[63]Marc S. Lavine, Numan Waheed, and Gregory C. Rutledge. Molecular dynamics simulation of orientation and crystallization of polyethylene during uniaxial extension. *Polymer*, 44(5):1771 – 1779, 2003.

[64]Min Jae Ko, Numan Waheed, Marc S. Lavine, and Gregory C. Rutledge. Characterization of polyethylene crystallization from an oriented melt by molecular dynamics simulation. *The Journal of Chemical Physics*, 121(6):2823–2832, 2004.

[65]T. C. Ionescu, C. Baig, B. J. Edwards, D. J. Keffer, and A. Habenschuss. Structure formation under steady-state isothermal planar elongational flow of n-eicosane: A comparison between simulation and experiment. *Phys. Rev. Lett.*, 96:037802, Jan 2006.

[66]A. Jabbarzadeh and R.I. Tanner. Crystallization of alkanes under quiescent and shearing conditions. *Journal of Non-Newtonian Fluid Mechanics*, 160(1):11 – 21, 2009. Complex flows of complex fluids.

[67]I. Dukovski and M. Muthukumar. Langevin dynamics simulations of early stage shish-kebab crystallization of polymers in extensional flow. *The Journal of Chemical Physics*, 118(14):6648–6655, 2003.

[68]Chunggi Baig and Brian J. Edwards. Atomistic simulation of crystallization of a polyethylene melt in steady uniaxial extension. *Journal of Non-Newtonian Fluid Mechanics*, 165(1718):992 – 1004, 2010. Proceedings of the 5th International Workshop on Non-Equilibrium Thermodynamics {IWNET} 2009.

[69]C. Baig and B. J. Edwards. Atomistic simulation of flow-induced crystallization at constant temperature. *EPL*, 89:36003, 2010.

[70]David A. Nicholson and Gregory C. Rutledge. Molecular simulation of flow-enhanced nucleation in n-eicosane melts under steady shear and uniaxial extension. *The Journal of Chemical Physics*, 145(24):244903, 2016.

[71]R S Graham. Understanding flow-induced crystallisation in polymers: a perspective on the role of molecular simulations. *Journal of Rheology*, 63(1):203–214, 2019.

[72]Muhammad Anwar, Joshua T. Berryman, and Tanja Schilling. Crystal nucleation mechanism in melts of short polymer chains under quiescent conditions and under shear flow. *The Journal of Chemical Physics*, 141(12):124910, 2014.

[73]Muhammad Anwar and Tanja Schilling. Crystallization of polyethylene: A molecular dynamics simulation study of the nucleation and growth mechanisms. *Polymer*, 76:307 – 312, 2015.

[74]Wolfgang Paul, Do Y. Yoon, and Grant D. Smith. An optimized united atom model for simulations of polymethylene melts. *The Journal of Chemical Physics*, 103(4):1702–1709, 1995.

[75]N. Waheed, M.J. Ko, and G.C. Rutledge. Molecular simulation of crystal growth in long alkanes. *Polymer*, 46(20):8689 – 8702, 2005.

[76]G. Ungar, J. Stejny, A. Keller, I. Bidd, and M. C. Whiting. The crystallization of ultralong normal paraffins: The onset of chain folding. *Science*, 229(4711):386–389, 1985.

[77]A W Lees and S F Edwards. The computer study of transport processes under extreme conditions. *Journal of Physics C: Solid State Physics Volume 5 Number 15*, 5, 1972.

[78]Thomas Soddemann, Burkhard Dünweg, and Kurt Kremer. Dissipative particle dynamics: A useful thermostat for equilibrium and nonequilibrium molecular dynamics simulations. *Phys. Rev. E*, 68:046702, Oct 2003.

[79]H J Limbach, A Arnold, B A Mann, and C Holm. ESPResSo—an extensible simulation package for research on soft matter systems. *Computer Physics Communications*, 174(9):704–727, 2006.

[80]Jing Cao and Alexei E. Likhtman. Simulating startup shear of entangled polymer melts. *ACS Macro Letters*, 4(12):1376–1381,

2015.

[81] Nobuyuki Iwaoka, Katsumi Hagita, and Hiroshi Takano. Estimation of relaxation modulus of polymer melts by molecular dynamics simulations: Application of relaxation mode analysis. *Journal of the Physical Society of Japan*, 84(4):044801, 2015.

[82] Richard S. Graham, Alexei E. Likhtman, Tom C. B. McLeish, and Scott T. Milner. Microscopic theory of linear, entangled polymer chains under rapid deformation including chain stretch and convective constraint release. *Journal of Rheology*, 47:1171, 2003.

[83] Martin Krger. Shortest multiple disconnected path for the analysis of entanglements in two- and three-dimensional polymeric systems. *Computer Physics Communications*, 168(3):209 – 232, 2005.

[84] Sachin Shanbhag and Martin Krger. Primitive path networks generated by annealing and geometrical methods: insights into differences. *Macromolecules*, 40(8):2897–2903, 2007.

[85] Robert S. Hoy, Katerina Foteinopoulou, and Martin Kröger. Topological analysis of polymeric melts: Chain-length effects and fast-converging estimators for entanglement length. *Phys. Rev. E*, 80:031803, Sep 2009.

[86] Nikos Ch. Karayiannis and Martin Krger. Combined molecular algorithms for the generation, equilibration and topological analysis of entangled polymers: Methodology and performance. *International Journal of Molecular Sciences*, 10(11):5054–5089, 2009.

[87] J.D. Ferry. *Viscoelastic properties of polymers*. Wiley, 1961.

[88] Adrian Andriescu and Simon A.M. Hesp. Timetemperature superposition in rheology and ductile failure of asphalt binders. *International Journal of Pavement Engineering*, 10(4):229–240, 2009.

[89] Yannick Rouault and Kurt Kremer. Timetemperature and timedensity superposition in the simulation of rheological properties of polymers. *The Journal of Chemical Physics*, 111(7):3288–3293, 1999.

[90] Macabas P. H. P. and Demarquette N. R. Time-temperature superposition principle applicability for blends formed of immiscible polymers. *Polymer Engineering & Science*, 42(7):1509–1519, 2004.

[91] Anja Vananroye, Pieter Leen, Peter Van Puyvelde, and Christian Clasen. TTS in LAOS: validation of time-temperature superposition under large amplitude oscillatory shear. *Rheologica Acta*, 50(9):795–807, Oct 2011.

[92] Tamio Yamazaki. Breakdown of timetemperature superposition in a beadspring polymer melt near the glass transition temperature. *The Journal of Physical Chemistry B*, 118(50):14687–14694, 2014. PMID: 25485844.

[93] Paula Wood-Adams and Stphane Costeux. Thermorheological behavior of polyethylene:effects of microstructure and long chain branching. *Macromolecules*, 34(18):6281–6290, 2001.

[94] Ute Kener, Joachim Kaschta, and Helmut Mnstedt. Determination of method-invariant activation energies of long-chain branched low-density polyethylenes. *Journal of Rheology*, 53(4):1001–1016, 2009.

[95] Malcolm L. Williams, Robert F. Landel, and John D. Ferry. The temperature dependence of relaxation mechanisms in amorphous polymers and other glass-forming liquids. *Journal of the American Chemical Society*, 77(14):3701–3707, 1955.

[96] Raju V. R., Smith G. G., Marin G., Knox J. R., and Graessley W. W. Properties of amorphous and crystallizable hydrocarbon polymers. i. melt rheology of fractions of linear polyethylene. *Journal of Polymer Science: Polymer Physics Edition*, 17(7):1183–1195.

[97] Jan Wedekind, Reinhard Strey, and David Reguera. New method to analyze simulations of activated processes. *The Journal of Chemical Physics*, 126(13):134103, 2007.

[98] Maziar Derakhshandeh and SavvasG. Hatzikiriakos. Flow-induced crystallization of high-density polyethylene: the effects of shear and uniaxial extension. *Rheologica Acta*, 51(4):315–327, 2012.

[99] Kenny Jolley and Richard S. Graham. Flow-induced nucleation in polymer melts: a study of the go model for pure and bimodal blends, under shear and extensional flow. *Rheologica Acta*, 52(3):271–286, 2013.

[100] R. R. Lagasse and B. Maxwell. An experimental study of the kinetics of polymer crystallization during shear flow. *Polymer Engineering & Science*, 16(3):189–199, 1976.

[101] Emmanuelle Koscher and Ren Fulchiron. Influence of shear on polypropylene crystallization: morphology development and kinetics. *Polymer*, 43(25):6931 – 6942, 2002.

[102] Kenny Jolley and Richard S. Graham. A fast algorithm for simulating flow-induced nucleation in polymers. *Journal Of Chemical Physics*, 134:11, 2011.

[103] Rosalind Allen, Patrick Warren, and Pieter Ten Wolde. Sampling rare switching events in biochemical networks. *Phys Rev Lett*, 94(1):018104, 2005.